Determination of Cr:LiSAF crystals ablation thresholds on the 20 ps regime using a diagonal scan

Ricardo E. Samad, Sonia L. Baldochi and Nilson D. Vieira Jr
IPEN/CNEN-SP – Centro de Lasers e Aplicações
Av. Prof. Lineu Prestes 2242, 05508-000, São Paulo, SP, Brazil

ABSTRACT

The usual method to determine the ablation threshold of solid samples by ultrashort laser pulses is done by focusing the laser beam on the samples surface by a known lens, requires the knowledge of all the geometrical parameters (lens focus, beam propagation parameters, beam quality, sample position), and a series of measurements for different pulse energies. We present here a simpler method for determining ultrashort laser pulses ablation threshold for solid samples. The method uses a focusing lens, and requires only the knowledge of the pulse power, employing a diagonal translation of the sample through the laser beam waist, resulting in a pattern etched on the sample surface. The ablation threshold value is obtained measuring only one dimension of this pattern and a straightforward mathematical relation, There is no need to know any other geometrical parameter of the laser beam or of the lens used. The technique was employed to determine the ablation threshold of pure and Cr doped LiSAF samples for 20 picoseconds pulses, and a dependence with the Cr concentration was observed.

Keywords: laser ablation, ablation threshold, ultrafast phenomena, Cr:LiSAF, diagonal scan

1. INTRODUCTION

Ultrashort pulse laser ablation of solids is due to electron avalanche induced breakdown[1, 2] which occurs when seed electrons are accelerated in the laser field, producing other free electrons by collisions. The breakdown takes place when the plasma originated by the avalanche electrons reaches a critical density and transfers energy to lattice ions, which expand away from the surface after the pulse has passed. In dielectrics and semiconductors seed electrons are created from the valence band either by multiphoton ionization[1, 3, 4, 5] or by tunneling induced by the laser field[6, 7], depending on the magnitude of the local electric field[8]. In metals, the seed electrons are the conduction band free electrons. After the seed electrons are present, there is a metallization of the material, and the avalanche happens deterministically[2, 9, 10, 11] in the same way in all solid materials, that start to behave like metals[12, 13]. Due to this nonselective characteristic of ultrashort pulse ablation, the only material parameter needed to know to machine a specific material is its ablation threshold, I_t.

The customary method[14] for the ablation threshold determination consists in measuring the ablation area diameter of a TEM_{00} Gaussian beam[15] at various fluences, and fitting a function to the data. This requires the knowledge of all the geometrical experimental parameters (lens focal length, beam propagation law), the pulse energy and a series of measurements. This method is widely used for pulse widths under tens of picoseconds where there is no significant lateral diffusion of heat. If lattice heating occurs, the size of the damaged region will depend on thermal properties of the material, and this method can no longer be used.

We present here a simple method for measuring the ultrashort pulses ablation threshold of a solid sample. This method consists in etching a pattern in the surface of a sample scanned diagonally across the beam waist of a focused ultrashort pulse laser beam, and then measuring the maximum transversal dimension of this etched pattern. The only experimental parameter that should be known is the ultrashort pulse peak power. The method was applied to determine the ablation threshold for pure and Chromium doped LiSAF crystals, and a dependence of the ablation threshold with the Cr doping was observed.

Solid State Lasers XVI: Technology and Devices, edited by Hanna J. Hoffman, Ramesh K. Shori, Norman Hodgson,
Proc. of SPIE Vol. 6451, 64511C, (2007) · 0277-786X/07/$15 · doi: 10.1117/12.699156

2. THEORY

Our objective is to describe the geometry of an intensity dependent damage etched in a sample surface by ultrashort pulses from a Gaussian beam[15]. For this purpose, we consider a sample placed with its surface orthogonally to the Gaussian beam, at a position where ablation occurs. In cylindrical coordinates, the radial intensity distribution (power density) of a pulse in a Gaussian beam is given by[16]:

$$I(r,z) = \frac{2P_0}{\pi w(z)^2} e^{-2\frac{r^2}{w(z)^2}} \quad , \quad \int_0^{2\pi} d\theta \int_0^{\infty} rdrI(z,r) = P_0 \tag{1}$$

where P_0 is the pulse power, r and z are the beam radial and longitudinal coordinates; $w(z)$ is the beam radius where the intensity drops to $1/e^2$ of the peak, given by:

$$w(z) = w_0\left[1+\left(\frac{\lambda M^2 z}{\pi w_0^2}\right)^2\right]^{1/2} = w_0\left[1+\left(\frac{z}{z_0}\right)^2\right]^{1/2} \tag{2}$$

where λ is the laser wavelength, w_0 is the beam waist (beam minimum *radius*), M^2 is the beam quality factor and $z_0=\pi w_0^2/(\lambda M^2)$ is the beam confocal parameter. The beam waist w_0 is located at z=0, and $w(z)$ is symmetrical around this position.

In a particular material, the breakdown only occurs if the local electric field intensity exceeds the threshold value I_t. That means that the local intensity will reach the threshold for a radius $\rho(z)$, and that for smaller radii the ablation will occur. Substituting $\rho(z)$ and I_t in equation (1) and solving for $\rho(z)$ we obtain:

$$\rho(z) = \sqrt{\frac{w(z)^2}{2}\ln[\frac{2}{\pi w(z)^2}\frac{P_0}{I_t}]} \tag{3}$$

which describes the ablation profile border.

For powers above $P_{crit}=\frac{1}{2}e\pi w_0^2 I_t$, it can be demonstrated[17] that the ablation profile has two symmetric lobes, as shown in Figure 1, where expression (3) and the beam profile $w(z)$ (eq. (2)) are plotted along the longitudinal direction z. It can be seen in equation (3) that $\rho(z)$ is symmetric around z=0, and deriving this expression to find its maxima we determine that the lobe maximum radius, ρ_{max}, depends *only* on the laser power and on the material damage threshold, and in no other parameter as the lens used or the laser beam propagation geometry:

$$\rho_{max} = \sqrt{\frac{1}{e\pi}\frac{P_0}{I_t}} \approx 0.342\sqrt{\frac{P_0}{I_t}} \tag{4}$$

The maxima position, $\pm\chi$, the ablation profile limits, $\pm\chi$, and the minimum damage radius, ρ_{min}, al shown in Figure 1, depend on the beam propagation parameters and are discussed in details in our earlier work[17].

Isolating the threshold intensity from equation (4) we obtain:

$$I_t = \frac{P_0}{e\pi\rho_{max}^2} \cong 0.117\frac{P_0}{\rho_{max}^2} \tag{5}$$

This last expression for the ablation threshold intensity I_t is a simple one, depending only on two parameters: the maximum damage radius, ρ_{max}, and the laser power, P_0, readily measurable. The ablation fluence F_t is readily obtained by multiplying the threshold intensity I_t by the pulse duration.

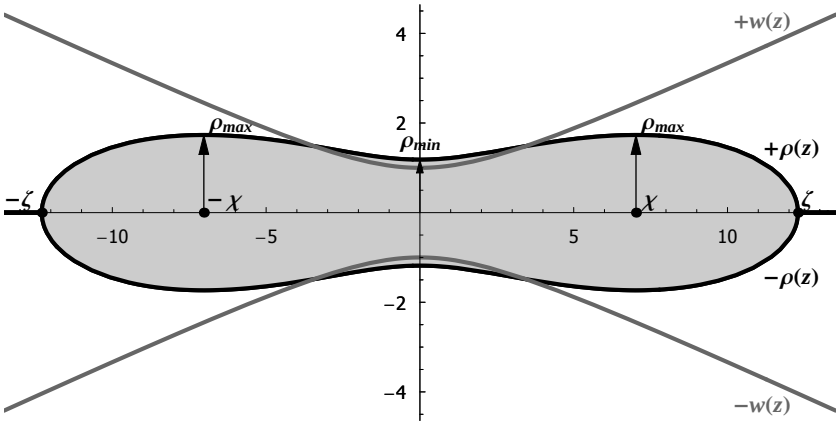

Figure 1. Ablation threshold profile for $P_0=6P_{crit}=e\pi w_0^2 I_t$. The beam radius at $1/e^2$ of peak intensity, $w(z)$, and the radius of the ablation spot, $\rho(z)$, where $I(\rho)=I_t$, are indicated. The shaded region is where ablation occurs. The longitudinal (z) and transversal axes are normalized by the confocal parameter z_0 and beam waist w_0, respectively.

To etch the ablation profile shown in Figure 1 in the surface of a sample, the ultrashort pulse laser beam, with known power, must be focused with a converging lens. The sample is then placed, with the beam normally to its surface, at a position where there is no ablation; the sample is then translated, diagonally to the beam (Figure 2), stopping the movement after the ablation ceases. If the ablation profile does not show two lobes, the scan must be repeated with a higher laser power or a stronger lens (tighter focus), which will provide power above the critical powerP_{crit} [17]. Once a damage profile with the two lobes is obtained, its maximum radius is measured and equation (5) is used to determine the ablation intensity threshold value, I_t.

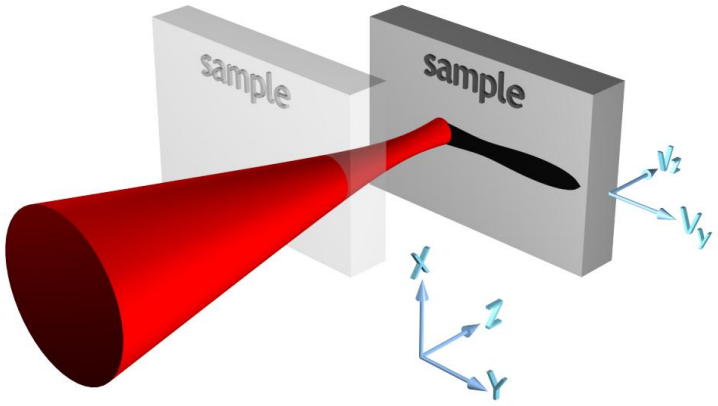

Figure 2. Ablation threshold determination under exposure to the laser beam. The black shape in the face of the sample is the ablation profile. The sample is translated diagonally through the beam waist, from the initial position at the left, to the final one at the right.

3. EXPERIMENTAL SETUP

Ultrashort pulses were utilized to determine the ablation threshold for 4 Cr:LiSAF samples. The first sample is a pure LiSAF one, two of the samples have 1mol% of Cr^{3+}, and the last sample has 1.5mol% of Cr^{3+}. The pure and 1% Cr doped samples were grown in our laboratories at IPEN, and the 1.5 Cr doped one was grown by VLOC. An amplified Ti:Sapphire laser was used; the laser beam, containing 18.9 ps (FWHM) pulses, centered at 830 nm, at 1 kHz repetition rate, was focused by a 20 cm convergent lens, and the samples were fixed to a x-y translation table controlled by

computer. The samples were moved diagonally to the laser beam by y=10 mm and z=60 mm, through its waist, at constant speeds v_y=1 mm/s and v_z=6 mm/s. In each sample, ablation profiles were etched, vertically apart by 500 μm, at different pulse energies. The samples were observed under an optical microscope, were the maximum transversal dimensions of the profiles were measured to determine the ablation thresholds.

4. RESULTS AND DISCUSSION

In Figure 3 the ablation profiles etched by 18.9 ps pulses in the surface of a pure LiSAF sample, measured in an optical microscope, are shown. The vertical separation between the profiles is 500 μm, providing a scale to measure the maximum transversal dimension of the profiles. In Table 1 the transversal values measured, along with pulse energies and calculated ablation threshold are shown for the pure LiSAF sample, following the Figure 3 numbering.

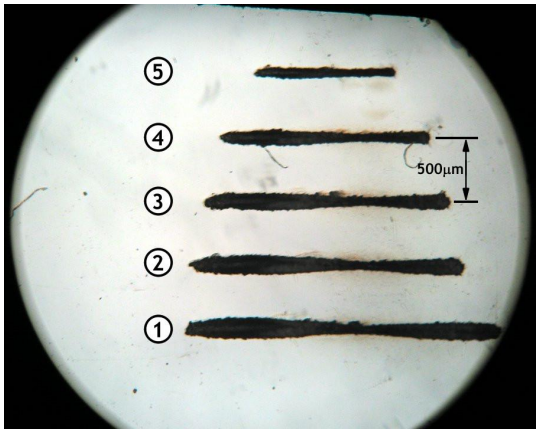

Figure 3. Optical microscope photograph used to determine the 18.9 ps ablation threshold of a pure LiSAF crystal.

Profile	ρ_{max} (μm)	E_p (μJ)	P (MW)	I_t (GW/cm^2)	F_t (J/cm^2)
1	79.8 ± 4,9	814 ± 9	43.4 ± 0.5	79.7 ± 9.8	1.50 ± 0.18
2	73.1 ± 4,8	723 ± 11	38.5 ±0.6	84.2 ± 11.1	1.58 ± 0.21
3	64.3 ± 4,7	587 ± 8	31.2 ±0.4	88.5 ± 13.1	1.66 ± 0.25
4	55.4 ± 4,6	447 ± 8	23.8 ±0.4	90.7 ± 15.3	1.71 ± 0.29
5	42.1 ± 4,6	279 ± 6	14.8 ± 0.3	98.0 ± 21.3	1.84 ± 0.11
		Average values		85.4 ± 5.7	1.61 ± 0.11

Table 1. Ablation threshold values measured for the pure LiSAF sample shown in Figure 3. The last line presents the average values for the ablation threshold intensity and fluence.

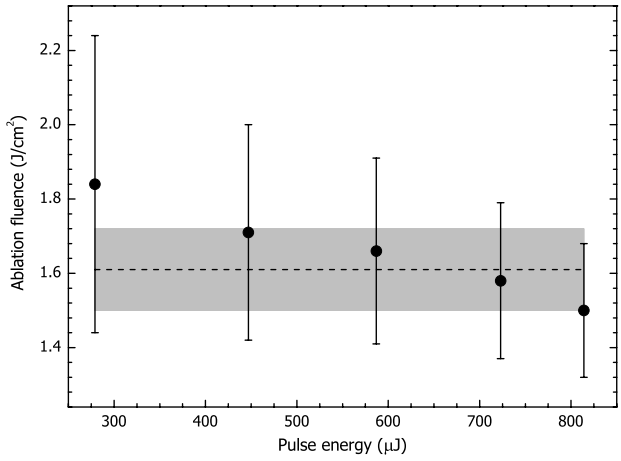

Figure 4. Ablation threshold fluence dependence on the pulse energy for the pure LiSAF sample. The dashed line is the ablation threshold average value from Table 1, and the shadowed area represents its standard deviation.

Figure 5 depicts an optical microscope photograph showing the profiles etched by 18.9 ps in the surface of a 1% Cr doped LiSAF sample by different energy pulses. The profiles are very similar to the ones etched in the pure LiSAF sample (Figure 3), and are also vertically separated by 500 μm.

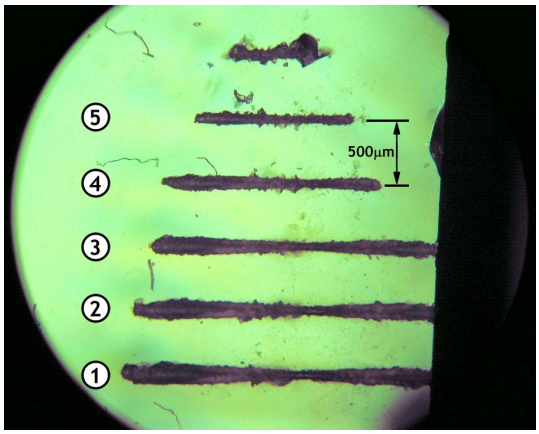

Figure 5. Optical microscope photograph used to determine the 18.9 ps ablation threshold of a 1mol% Cr doped LiSAF crystal.

Profile	ρ_{max} (μm)	E_p (μJ)	P (MW)	I_t (GW/cm^2)	F_t (J/cm^2)
1	80.5 ± 9.2	692 ± 13	36.8 ± 0,7	66.5 ± 15.4	1.25 ± 0.29
2	71.6 ± 4.8	584 ± 11	31.1 ± 0,6	71.0 ± 9.7	1.33 ± 0.18
3	62.4 ± 4.8	484 ± 11	25.7 ± 0,6	76.8 ± 11.8	1.44 ± 0.22
4	55.9 ± 4.7	344 ± 9	18.3 ± 0,5	68.5 ± 11.6	1.29 ± 0.22
5	44.7 ± 4.6	225 ± 5	12.0 ±0,3	70.0 ± 14.,5	1.32 ±0.27
		Average values		71.0 ± 5.4	1.33 ± 0.10

Table 2. Ablation threshold values measured for the Cr:LiSAF sample shown in Figure 5. The last line presents the average values for the ablation threshold intensity and fluence.

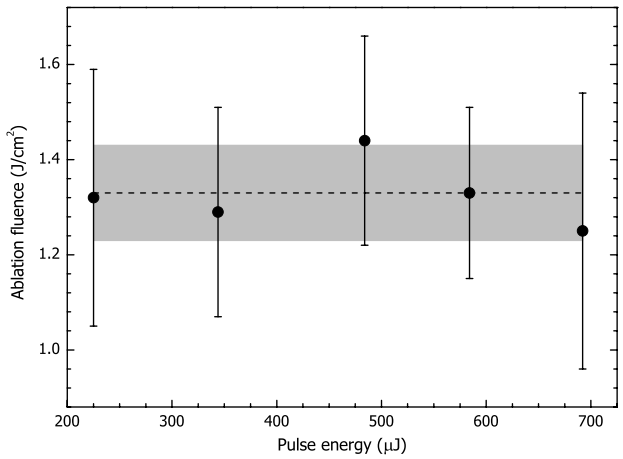

Figure 6. Ablation threshold fluence dependence on the pulse energy for the 1mol% Cr doped LiSAF sample. The dashed line is the ablation threshold average value, and the shadowed area represents its standard deviation.

The ablation threshold intensities and fluences were also determined for the two other samples (1% and 1.5% Cr doping) following the same procedure, and its values are shown in Table 3. In Figure 7 the fluence values are plotted as a function of the Cr^{3+} concentration.

Sample	Cr^{3+} doping (mol%)	I_t (GW/cm^2)	F_t (J/cm^2)
1	0	85.4 ± 5.7	1.61 ± 0.11
2	1	71.0 ± 5.4	1.33 ± 0.10
3	1	72.8 ± 4.7	1.37 ± 0.09
4	1.5	81.4 ± 6.6	1.53 ± 0.12

Table 3. ablation threshold fluences (F_t) and threshold intensities (I_t), determined for each sample.

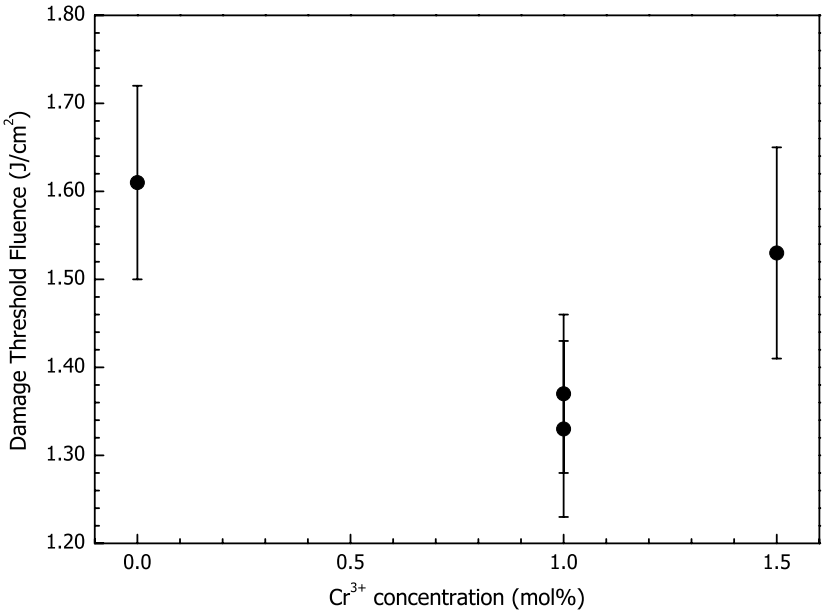

Figure 7. ablation threshold fluences plotted as a function of the Cr3+ doping of the samples.

In the results shown in Table 3 and in Figure 7, it can be seen that the ablation threshold decreases with the increase of Chromium concentration in the samples. This is an expected result, since the insertion of a dopant in the host creates absorptions that can start the ablation process. Even if these absorptions are residual in the laser wavelength, in the ultrashort pulse regime they are enough to lower the ablation threshold by the mechanisms described in the introduction. Besides, the dopant introduction in the crystal matrix distorts the crystal structure, creating local stresses that degrade the host mechanical properties. The unexpected results is that the higher Chromium concentration (1.5mol%) sample has a higher ablation threshold than the 1mol% samples. However, the lower Cr content samples, grown at our laboratories, have not gone through an annealing process, which would reduce stresses remaining from the growth process. The higher Cr concentration sample, grown by VLOC, has probably passed through an annealing process, minimizing tensions and increasing the ions bond energies to the structure, what improves the crystal mechanical properties[18]. This additional energy results in a rise in the ablation threshold. The samples grown at IPEN will go through an annealing process, that is expected to increase the ions bonding energies, and then their ablation thresholds will be measured again to check if the crystals mechanical properties that contribute to the ablation process are improved.

5. CONCLUSIONS

We developed a simple method to determine the ablation threshold of solid samples in the ultrashort laser pulse regime. The method is easily implemented, an requires only the knowledge of the laser power. Using this method, we have determined the ablation threshold of pure and Chromium doped LiSAF samples. We observed a decrease of the ablation threshold with the Cr^{3+} concentration increase, that can be explained by residual absorption and mechanical stress, both resulting from the Cr^{3+} introduction on the crystal. Future measurements are planned to verify if the crystal ablation threshold can be increased by annealing processes.

ACKNOWLEDGMENTS

The authors thank FAPESP for financial support under the grant 00/15135-9.

REFERENCES

1. N. Bloembergen, "Laser-Induced Electric Breakdown in Solids", *IEEE J. Quantum Elec.* **10**, 375-386 (1974).
2. D. Du, X. Liu, G. Korn, J. Squier and G. Mourou, "Laser-induced breakdown by impact ionization in SiO_2 with pulse widths from 7 ns to 150 fs", *Appl. Phys. Lett.* **64**, 3071-3073(1994).
3. M. D. Perry, B. C. Stuart, P. S. Banks, M. D. Feit, V. Yanovsky and A. Rubenchik, "Ultrashort-pulse laser machining of dielectric materials", *J. Appl. Phys.* **85**, 6803-6810 (1999).
4. W. Kautek, J. Krüger, M. Lenzner, S. Sartania, C. Spielmann and F. Krausz, "Laser ablation of dielectrics with pulse durations between 20 fs and 3 ps", *Appl. Phys. Lett*. **69**, 3146-3148(1996).
5. B. C. Stuart, M. D. Feit, A. M. Rubenchik, B. W. Shore and M. D. Perry, "Laser-induced Damage in Dielectrics with Nanosecond to Subpicosecond Pulses", *Phys. Rev. Lett.* **74**, 2248-2251 (1995).
6. M. Lenzner, J. Krüger, S. Sartania, Z. Cheng, Ch. Spielmann, G. Mourou, W. Kautek and F. Krausz, "Femtosecond Optical Breakdown in Dielectrics", *Phys. Rev. Lett.* **80**, 4076-4079 (1998).
7. A. P. Joglekar, H. Liu, G. J. Spooner, E. Meyhöffer, G. Mourou and A. J. Hunt, "A study of the deterministic character of optical damage by femtosecond laser pulses and applications to nanomachining", *Appl. Phys. B – Lasers and Optics* **77**, 25-30 (2003).
8. L. V. Keldysh, "Ionization in the field of a strong electromagnetic wave", *Sov. Phys. JETP* **20**, 1307-1314 (1965).
9. M. Bass and D. W. Fradin, "Surface and Bulk Laser-Damage Statistics and the Identification of Intrinsic Breakdown Processes", *IEEE J. Quantum Elec.* **9**, 890-896 (1973).
10. R. T. Brown and D. C. Smith, "Laser-induced gas breakdown in the presence of preionization", *Appl. Phys. Lett.* **22**, 245-247 (1973).
11. M. Bass and H. H. Barrett, "Laser-induced Damage Probability at 1.06 μm and 0.69 μm", *Appl. Opt.* **12**, 690-699 (1973).
12. S. Nolte, C. Momma, H. Jacobs, A. Tünnermann, B. N. Chichkov, B. Wellegehausen, and H. Welling, "Ablation of metals by ultrashort laser pulses", *J. Opt. Soc. Am. B* **14**, 2716-2722 (1997).
13. E. G. Gamaly, A. V. Rode, B. Luther-Davies and V. T. Tikhonchuk, "Ablation of solids by femtosecond lasers: Ablation mechanism and ablation thresholds for metals and dielectrics", *Phys. Plasmas* **9**, 949-957 (2002).
14. J. M. Liu, "Simple technique for measurements of pulsed Gaussian-beam spot sizes", *Opt. Lett.* **7**, 196-198 (1982).
15. H. Kogelnik and T. Li, "Laser Beams and Resonators" *Appl. Opt.* **5**, 1550-1567 (1966).
16. D. R. Hall and P. E. Jackson, "The physics and technology of laser resonators", *IOP Publishing*, 1989, Chap. 1.

17. R. E. Samad and N. D. Vieira Jr, "Geometrical Method for Determining the Surface Damage Threshold for Femtosecond Laser Pulses", *Laser Phys.* **16**, 336-339 (2006).

18. J. J. De Yoreo, L. J. Atherton and D. H. Roberts, "Elimination of scattering centers from Cr:$LiCaAlF_6$", *J. Crystal Growth* **113**, 691-697 (1991).